Nuclear structure studies of ^{70}Zn from g-factor and lifetime measurements

D. Mücher,[1] G. Gürdal,[2] K.-H. Speidel,[3] G. J. Kumbartzki,[2] N. Benczer-Koller,[2] S. J. Q. Robinson,[4] Y. Y. Sharon,[2]
L. Zamick,[2] A. F. Lisetskiy,[5] R. J. Casperson,[6] A. Heinz,[6] B. Krieger,[2] J. Leske,[7] P. Maier-Komor,[8]
V. Werner,[6] E. Williams,[6] and R. Winkler[6]

[1]*Institut für Kernphysik, Universität zu Köln, Zülpicher Str. 77, D-50937 Köln, Germany*
[2]*Department of Physics and Astronomy, Rutgers University, Piscataway, New Jersey 08854, USA*
[3]*Helmholtz-Institut für Strahlen- und Kernphysik, Universität Bonn, Nussallee 14-16, D-53115 Bonn, Germany*
[4]*Physics Department, Millsaps College, Jackson, Mississippi 39210, USA*
[5]*Department of Physics, University of Arizona, Tucson, Arizona 85721, USA*
[6]*A. W. Wright Nuclear Structure Laboratory, Yale University, New Haven, Connecticut 06520, USA*
[7]*Institut für Kernphysik, Technische Universität Darmstadt, Schlossgartenstr. 9, D-64289 Darmstadt, Germany*
[8]*Physik-Department, Technische Universität München, James-Franck-Str., D-85748 Garching, Germany*

The g factors and mean lifetimes of several short-lived low-lying states in $^{70}_{30}$Zn$_{40}$ have been measured using the techniques of projectile Coulomb excitation in inverse kinematics combined with transient magnetic fields and the Doppler-shift attenuation method. The present results have been interpreted within the framework of large-scale shell-model calculations that include the $g_{9/2}$ orbital.

I. INTRODUCTION

In current nuclear structure studies, fp-shell nuclei in general, and the Zn isotopes in particular, have attracted much attention due to the availability of new experimental g factors and $B(E2)$ values [1–7] as well as large-scale shell-model calculations. Among the interesting questions that have been considered are the changes in nuclear structure as the neutron number N increases toward and beyond the $N = 40$ subshell closure.

The magnetic moments of the 2^+_1 states have been determined in many $_{30}$Zn, $_{32}$Ge, and $_{34}$Se isotopes. These data have shed light on the proton and neutron configurations in the wave functions of the 2^+_1 states. Measurements of the magnetic moments of states with higher spins would indicate the evolution of the structure of these nuclei as a function of energy and spin, as well as proton and neutron numbers. For example, the wave functions of higher-spin states are generally more sensitive to contributions from high-j orbitals. It has also been suggested that some higher-lying 2^+ states may have mixed symmetry, a manifestation of a different structure [8,9]. In spite of the advantages of the transient field/Coulomb excitation technique in inverse kinematics, the measurements of the magnetic moments of the higher lying 4^+ and 3^- states remain challenging due to the weak excitation of the states and the smaller alignment of the initial spins. These data have been reviewed in Refs. [10,11] and in several articles on the Zn isotopes [1,3,4,12–14].

A major issue in the interpretation of the data relates to the extent of the contributions of neutron excitations to the $g_{9/2}$ orbital, for which the Schmidt value of the g factor is $g(g_{9/2}) = -0.425$. The g factor of the 4^+_1 state in the lighter Zn isotopes has been seen as a good indicator of possible $(g_{9/2})_\nu$ contributions.

The $g(4^+_1)$ factors in ^{64}Zn and ^{66}Zn, $g(4^+_1) = +0.53(16)$ [13] and $g(4^+_1) = +0.65(20)$ [4], respectively, can be ex-

plained without involving excitations to the $g_{9/2}$ orbital. But two experimental results for the $g(4^+_1)$ of ^{68}Zn yielded the negative values of $-0.4(2)$ [13] and $-0.3(3)$ [3], respectively, requiring dominant $(g_{9/2})_\nu$ contributions to the 4^+_1 wave function. However, a later measurement yielded a positive value of $g(^{68}$Zn, $4^+_1) = +0.6(3)$ [5], in agreement with the results of large-scale full-fp shell-model calculations that did not include the $g_{9/2}$ orbital. The inconsistency in the data should be clarified by further independent measurements.

In view of these observations, a measurement of $g(^{70}$Zn, $4^+_1)$ would extend the systematics in this mass region, investigate the robustness of the closures of the $N = 40$ subshell and the $Z = 28$ major shell, and help to clarify the role of the $g_{9/2}$ nucleons as N increases toward $N = 40$.

In a simple shell-model picture, the ground state of $^{70}_{30}$Zn$_{40}$ has a closed $N = 40$ neutron subshell and two valence $p_{3/2}$ protons, coupled to zero, beyond the closed $Z = 28$ proton shell. The 4^+_1 state wave function can be obtained by exciting one or two of the valence protons to the $f_{5/2}$ level and/or by exciting neutrons across the $N = 40$ barrier to the $g_{9/2}$ orbital or protons across the $Z = 28$ shell gap.

Currently, there is only sparse spectroscopic data on ^{70}Zn. Many transition γ rays are very nearly degenerate, few state lifetimes have been measured, and only the $g(2^+_1)$ value has been determined [1]. The present experiment aims to clarify the energy-level scheme, to reconfirm the $g(2^+_1)$ value, and to measure the $g(4^+_1)$ and $g(2^+_2)$ factors. The experiment will also determine the lifetimes of several low-lying excited states, thus providing the associated $B(E2)$ values. A partial level scheme, as presented in Ref. [15] and augmented with data from this experiment, is shown in Fig. 1. There are other interesting features of the ^{70}Zn low-lying excited states that should be further investigated. This spectrum exhibits some vibrational features, namely almost degenerate 4^+_1 and 2^+_2 states at about twice the excitation energy of the 2^+_1 state; however, the energy
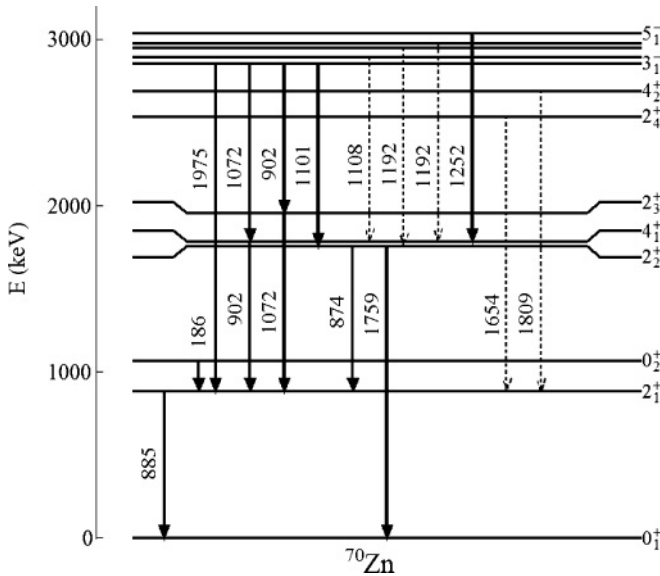
FIG. 1. Low-energy level scheme and γ transitions in ^{70}Zn as presented in Ref. [15] with additional data from the present experiment. Only γ rays observed in this experiment are included. The dotted lines represent weaker transitions.

of the 0_2^+ state is significantly lower. The systematics of the low-lying 0_2^+ states in the Zn, Ge, and Se isotope chains exhibit a drop in the 0_2^+ excitation energy at $N = 40$ and a rise for $N = 42$. For the ^{70,72,74}Ge nuclei the behavior of the 0_2^+ state as a function of N has been associated with both neutron and proton excitations to the $g_{9/2}$ intruder orbital [8]. The 3_1^- state at 2.859 MeV corresponds to 3_1^- levels in other nuclei that are commonly assumed to be associated with octupole vibrations [16,17]. Thus, the magnitudes and ratios of $B(E2)$ values and g factors are of special interest for comparison with predictions of calculations for either single-particle excitations or vibrations.

There are other theoretical motivations for more extensive studies of ^{70}Zn. Several large-scale shell-model calculations have been carried out to explain the experimental $B(E2)$ values and g factors of the even Zn isotopes. These have used different closed cores [^{40}Ca or ^{56}Ni], different shell-model spaces, such as the full fp or the $p_{3/2}f_{5/2}p_{1/2}g_{9/2}$ spaces, and different interactions, such as the KB3G [18] or the G-matrix formalism with the CD-Bonn [19] potential. Recent calculations for the Zn isotopes by F. Nowacki [1] used a ^{48}Ca core and included the $g_{9/2}$ neutrons that played an increasingly important role as N increased. In some shell-model calculations, deviations from the experimental data were found for the heaviest Zn isotopes and were attributed to the omission of excitations from the ^{56}Ni core. In the present article, for ^{70}Zn, the standard fp-shell interactions in the full fp space with a ^{40}Ca core [1], were initially utilized, allowing possible excitations from $f_{7/2}$ shell. Subsequently, the JJ4B interaction [20] in the $p_{3/2}f_{5/2}p_{1/2}g_{9/2}$ space with a ^{56}Ni core was used. The comparison of the results of these two calculations for ^{70}Zn with the experimental data will explicitly indicate, for this nucleus, the relative importance of excitations from the $f_{7/2}$ shell and to the $g_{9/2}$ intruder orbital.

II. EXPERIMENTAL DETAILS AND ANALYSIS

In the present experiment a beam of isotopically pure ^{70}Zn ions was accelerated to energies of 180 or 200 MeV at the ESTU Tandem accelerator of the Wright Nuclear Structure Laboratory (WNSL) at Yale University. Beams of about 1 pnA were obtained by using enriched ^{70}ZnO in the ion source of the accelerator. A multilayered target, with 0.46 mg/cm^2 natural carbon deposited on a 3.61 mg/cm^2 gadolinium layer, evaporated on a 1.6 mg/cm^2 tantalum foil, backed by a 4.2 mg/cm^2 copper layer, was used. Thin ($\sim$5.0 μg/cm^2) layers of natural titanium were added between the carbon and gadolinium, and also between the tantalum and copper, to provide good adherence of these elements to each other.

The target was cooled to temperatures of about 70 K – 80 K using a closed-cycle refrigerator. It was magnetized to saturation in an external field of 0.09 T. The external field was alternated in the up and down directions with respect to the γ-ray detection plane every 162 s. The magnetization, M, of the target was measured as a function of the temperature in the range between 25 K and 150 K in an AC magnetometer [21]. It was found to be $M = 0.1960$ T and approximately constant from 60 K to 120 K.

The ^{70}Zn nuclei were Coulomb excited in collisions with the carbon target nuclei in inverse kinematics. The selection of a beam energy of 200 MeV, which is 20 MeV above the Coulomb barrier, was determined by the desire to enhance the excitation of the 4_1^+ state. However, the simultaneous excitation of several higher energy states, especially the 3_1^- state, added to the complexity in the γ spectra. A run was carried out with a beam of 180 MeV to allow for a comparison with spectra where fewer states were excited.

The Coulomb-excited Zn nuclei traversed the gadolinium layer of the target at mean velocities of 6.4 v_0, where $v_0 = e^2/\hbar$. The spins of the states of interest were aligned by the Coulomb-excitation process and precessed in the transient field (TF) while traversing the gadolinium foil. The nuclei were ultimately stopped in the hyperfine-interaction-free environment of the copper backing. The beam ions passing through the composite target were stopped in an additional copper foil (placed behind the target) that was transparent to the fast carbon recoils.

The γ rays emitted from the excited states were detected together with the forward-scattered particles. Four HP-Ge clover detector modules, used for γ detection, were placed in a plane perpendicular to the magnetization direction at a distance of 13.2 cm from the target. A clover module contains four Ge crystals, each with about 28% relative efficiency. Compton-scattered γ rays within a clover were added back for a total relative efficiency of about 150%. The detectors were shielded by a triple absorber layer of Pb/Cd/Cu to reduce the low-energy γ-ray rate.

Because a clover detector is made up of four independent segments, it is advantageous to analyze the data of each segment separately to take advantage of the better angular resolution and the reduced Doppler broadening of γ lines. Two segments (Ge crystals) of a clover module are located at the same angles θ with respect to the beam direction in the reaction plane. "Splitting" each clover into halves creates

two four-detector sets for the analysis. At the given target-detector distance the effective angle separation of the clover halves is 15.4°, placing the new detectors at angles of $\theta = \theta$(clover) $\pm$ 7.7°. The separation angle was derived by fitting the 0.885-MeV data (corresponding to the $2_1^+ \rightarrow 0_1^+$ transition) from all the individual clover segments, taken at three clover settings and corrected for relative efficiencies, to the angular distribution function and minimizing the χ^2 by varying the separation angle. The Compton add-back for each segment was performed by attributing multiple γ events to the segment with the highest γ-ray energy.

An additional Ge detector with 25% relative efficiency was placed at 0° with respect to the beam axis. The purpose of this detector was to measure the lifetimes of the excited states by the Doppler-shift attenuation method (DSAM). Unfortunately, the particle-γ-coincidence spectrum had low statistics that limited its usefulness.

Particles were recorded in a Canberra PIPS Si detector of 300-mm^2 area and 100-μm depletion layer, positioned 18 mm downstream of the target and subtending an angle of $\pm 28°$. The energy and time information of every "singles" event in any detector was determined directly from the preamplifier signals in digitizing pulse processors from XIA [22] and stored on disk. From these data, "coincident events" were selected and recorded in event files for further sorting.

III. ANALYSIS AND RESULTS

A. Energy-level diagram

A particle spectrum, taken in coincidence with all the γ rays, is shown in Fig. 2. The peak structures shown refer to ^{12}C ions emitted from the carbon layer and, at slightly lower energies, to α particles. These α particles result from the breakup into two α particles of the ^{8}Be nuclei that remain after an α transfer from ^{12}C to the ^{70}Zn projectiles, forming ^{74}Ge. A particle-γ-coincidence spectrum, obtained in one segment of a clover detector located forward with respect to the beam direction and gated on the ^{12}C ions, is shown in Fig. 3. An
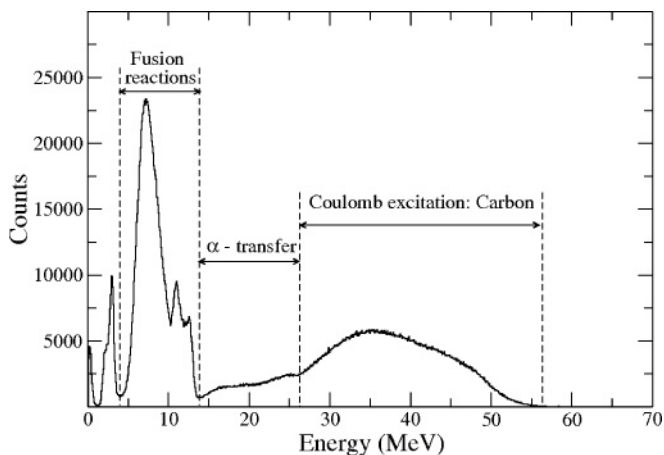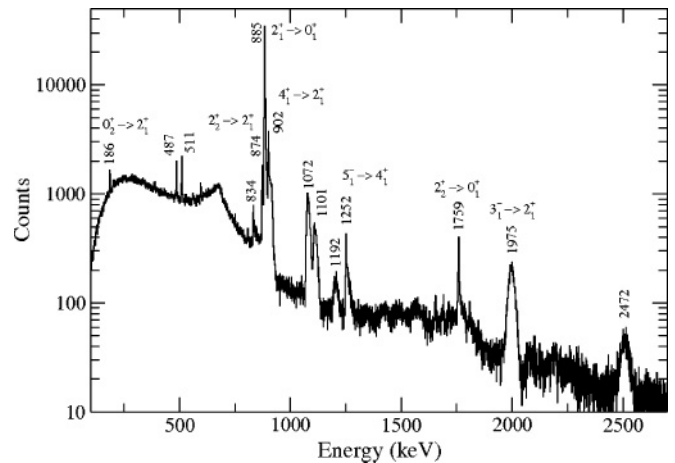

FIG. 3. The γ coincidence spectrum of ^{70}Zn, observed in a forward clover detector, gated by carbon ions. The fully shifted transitions are labeled with their corresponding rest energies.

analysis of ^{74}Ge data was not attempted because of a lack of statistics.

The level scheme shown in Fig. 1 displays only the γ rays observed in this experiment. This scheme is in partial agreement with the proposed energy level diagrams published in the literature [15] but differs in some essential ways. The difficulty in reconciling different proposed energy level schemes arises from the accidental degeneracy of several transitions, such as two at 0.902 MeV ($3_1^- \rightarrow 2_3^+$ and $4_1^+ \rightarrow 2_1^+$) and two at 1.072 MeV ($3_1^- \rightarrow 4_1^+$ and $2_3^+ \rightarrow 2_1^+$). The Coulomb excitation of heavy ions by a light target, used in this experiment, provides additional information in the form of excited nuclei recoiling at appreciable velocities. Short-lived states with lifetimes of less than 0.5 ps decay completely in flight and are fully Doppler shifted. The mean decay velocity is determined from the energies measured at various detector angles. The γ rays from the 3_1^- state at 2.883 MeV should all exhibit the same mean decay velocity. Although this observation is true for the $3_1^- \rightarrow 2_1^+$, 1.975-MeV, and the $3_1^- \rightarrow 2_2^+$, 1.101-MeV, transitions, the 1.072-MeV transition, also attributed as coming from the 3_1^- state, has a distinctly lower mean decay velocity, as shown in Fig. 4. The peak shifts for a forward- and a backward-placed γ detector are indicated by the arrows. Because the energies of the γ lines are close, different shifts represent different decay velocities. The average decay velocity of the 1.072-MeV transition is lower, indicating that most of these γ rays depopulate a different state, which decays at a later time than the 3_1^- state. The bulk, if not all, of this transition is attributed here to the $2_3^+ \rightarrow 2_1^+$ decay.

Similarly, the degenerate 0.902-MeV transition exhibits a fast-decaying component (fully Doppler shifted) with a decay velocity in agreement with a decay from the 3_1^- state. This 902-keV component is shown in Fig. 5. It has a different angular distribution and impedes the integration of the total line shape of the $4_1^+ \rightarrow 2_1^+$ transition of interest.

A possible 0.887-MeV ($2_3^+ \rightarrow 0_2^+$) transition cannot be resolved from the ($2_1^+ \rightarrow 0_1^+$) ground-state transition. A fully shifted 2.472-MeV transition was observed in this experiment,
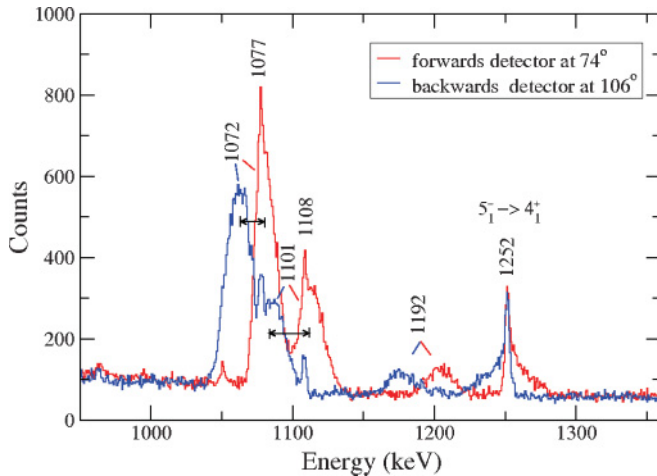

FIG. 2. A particle coincidence spectrum obtained with the Si detector at 0°.

FIG. 4. (Color online) Excerpt of the γ coincidence spectrum for the fully shifted 1072- and 1101-keV γ lines, shown for a forward detector and a backward detector. The picture shows the different Doppler shifts of the 1072- and the 1101-keV transitions. The small, sharp, γ lines are identified as the $2_1^+ \to 0_1^+$ transition in ^{68}Zn (1077 keV) and possibly the $6_1^+ \to 4_1^+$ transition in ^{70}Zn (1108 keV).

as shown in Fig. 3. This transition could not be found in the published level schemes of ^{70}Zn and could not be placed in the level scheme, but a v/c analysis suggests that this transition belongs to the ^{70}Zn nucleus.

B. Angular correlations

Angular correlation measurements are necessary to establish level spins as well as the slopes of the correlations that enter into the determination of the g factors obtained from precession measurements.
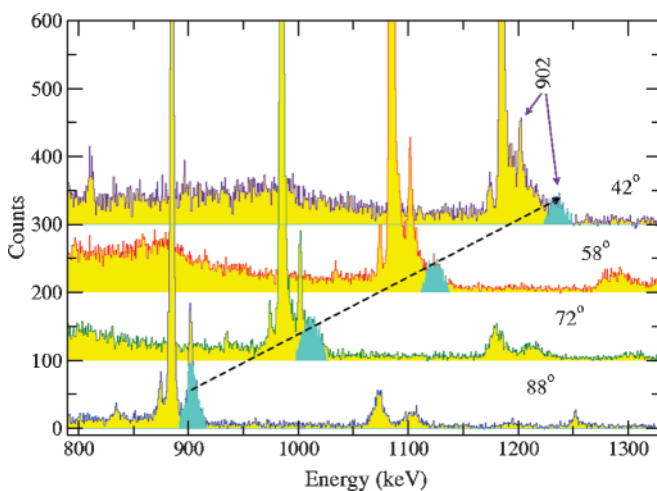

FIG. 5. (Color online) Expanded region of the γ coincidence spectrum near the dominating $2_1^+ \to 0_1^+$ transition for forward-placed clover segments at the indicated angles. The sharp line at 902 keV, which displays some line shape, corresponds to the decay of the 4_1^+ state. The broad, fully Doppler-shifted, peaks, connected by the dashed line, are attributed to the $3_1^- \to 2_3^+$ transition.

In general, the slope of the particle-γ angular correlation is obtained by measuring coincidence spectra for several particle γ-ray angles [10]. However, due to the limited beam time, it becomes practical to extract the parameters of the angular correlation from the anisotropy data, namely from the ratios of yields at only two angles. Anisotropy ratios can be formed from the efficiency-corrected precession data (summed over both magnetic field directions). The relative efficiencies of the clover segments were measured using a ^{152}Eu source at the target position. The slopes of the angular correlations were obtained from the anisotropy ratios in the manner detailed in Ref. [14].

C. Lifetime measurements

There are only few published measurements of lifetimes for the low-lying levels in ^{70}Zn, namely those of the 2_1^+, 2_2^+, and 0_2^+ states. In this experiment, lifetimes of several states were measured by the DSAM, as described in Ref. [1], using the computer code LINESHAPE [23].

Because the clover detectors have much higher statistics than the $0°$-γ detector, their data were also used for the line-shape analysis. Most of the data were taken with the clover detectors located at $\pm66°$ and $\pm114°$, forward and backward with respect to the beam direction, at angles where the precession measurements, taken simultaneously, are optimized.

Well-resolved lines with a pronounced line shape as well as a stopped peak component were readily analyzed. The most difficult analysis was carried out on the partially unresolved line, the critical one at 0.902 MeV. As shown in Fig. 5, the broad feature at 0.902 MeV is most intense near $90°$, indicating a dipole transition. The sharp line at 0.902 MeV has an angular correlation corresponding to a quadrupole transition, as seen in the 180 MeV data, and thus was assigned to the $4_1^+ \to 2_1^+$ transition.

The analysis of the line shape shown in Fig. 6(a) was carried out for the $4_1^+ \to 2_1^+ \to 0_1^+$ cascade in the $0°$ detector, neglecting a small tail contribution of the 0.874-MeV $2_2^+ \to 2_1^+$ transition. The lifetime of the 2_1^+ state was set equal to the literature value and kept constant in the fit. The fully Doppler-shifted and broad 0.902-MeV component depopulating the 3_1^- state is, because of its angular distribution, suppressed at $0°$ and peaks at 0.955 MeV. The lifetime result for the 4_1^+ state shown in Fig. 6(a) was corroborated in fits of clover data taken at $58.3°$ and at a beam energy of 180 MeV. The results are displayed in Table I.

D. Precession measurements

The spin precession in a magnetic field is measured as a rotation of the angular distribution of γ rays with respect to the direction of the external magnetic field that polarizes the gadolinium foil.

For the measurement of the precession, four detectors have traditionally been used. Detectors 1 and 4 are placed at backward angles relative to the beam direction
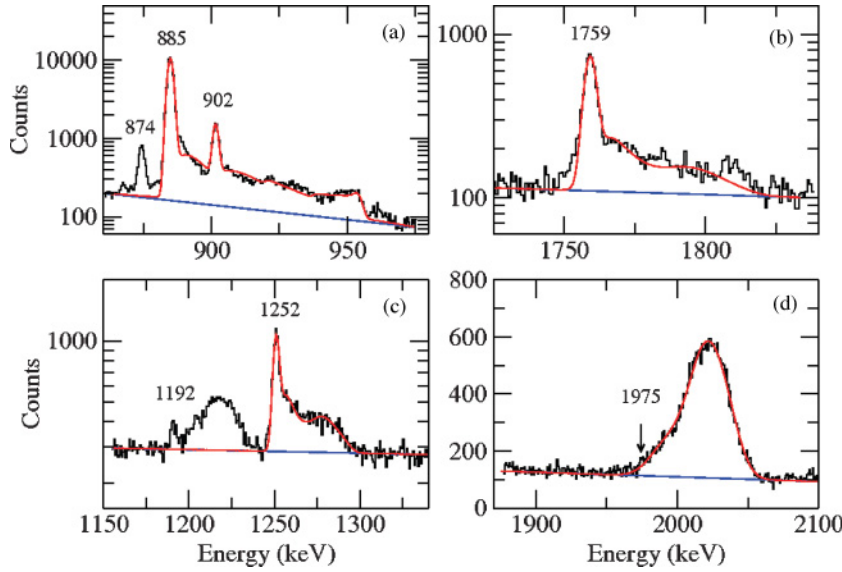
FIG. 6. (Color online) Line-shape fits for (a) the $4_1^+ \to 2_1^+ \to 0_1^+$ cascade observed in the 0° detector, (b) the $2_2^+ \to 0_1^+$, (c) the $5_1^- \to 4_1^+$, and (d) the $3_1^- \to 2_1^+$ transitions, all observed at 58.3° with respect to the beam direction.

($\theta = \pm 114°$), while detectors 2 and 3 are placed at forward angles ($\theta = \pm 66°$).

The precession angle $\Delta\theta$ is derived from the expression $\Delta\theta = \epsilon/S = [(\rho - 1)/(\rho + 1)]/S$, where $\rho = \sqrt{\rho_{14}/\rho_{23}}$ and $\rho_{ij} = \sqrt{N_i^{\uparrow} N_j^{\downarrow}/N_j^{\uparrow} N_i^{\downarrow}}$ for $i, j = 1, 2, 3, 4$. Here N is the counting rate for a transition in any one detector for a given direction of the magnetic field. The logarithmic slope S of the angular correlation $W(\theta)$ is given by $S = (1/W)(dW/d\theta)$. As described above, this experiment uses two sets of four detectors at angles of $\theta = \pm 58.3°, \pm 121.7°$, and $\theta = \pm 73.7°, \pm 106.3°$.

The g factor is extracted from the spin precession angle

$$\Delta\theta = -\frac{g\mu_N}{\hbar} \int_{t_{\mathrm{in}}}^{t_{\mathrm{out}}} B_{\mathrm{TF}}[v(t), Z] \cdot e^{-t/\tau} dt \qquad (1)$$

by dividing the observed precession by the calculated value of $\Delta\theta$ for $g = 1$. In this calculation, B_{TF}, the transient field, is a function of both the velocity v and the atomic number Z of the projectile ions; τ is the mean lifetime of the state being considered; and t_{in} and t_{out}, respectively, are the mean entrance and exit times of the ions into and out of the ferromagnetic layer. The value of B_{TF} was derived from the

TABLE I. Summary of lifetimes for states of excitation energy E_x measured in this work.

E_x (MeV)	I^{π}	τ(ps) [Ref.]	τ(ps) (this work)
0.885	2_1^+	5.3(3) [1]	–[a]
1.068	0_2^+	5628(289) [15]	
1.759	2_2^+	0.35(+35, −17) [15]	1.9(3)
1.786	4_1^+		1.9(2)
2.859	3_1^-		0.29(2)
3.038	5_1^-		1.5(1)

[a]A unique fit to the mean lifetime of the 2_1^+ state was not obtained from the data in this experiment because of the partially overlapping 4_1^+ state, the feeding into the 2_1^+, and the correlations between the various parameters in the multiline fit.

Rutgers parametrization [24]. B_{TF} is directly proportional to the magnetization M of the ferromagnetic foil.

The data relevant to the precession analysis are shown in Table II. The slope for the $4_1^+ \to 2_1^+$ transition could not be determined from the data in this experiment due to the complexity of the spectrum. The values quoted in the table are derived from the measured slope in a previous experiment, carried out under similar conditions, on ^{68}Zn [5].

IV. DISCUSSION

The stable Zn nuclei span a region where collective effects compete with single-particle excitations. It was noted in Sec. I that the $^{70}_{30}$Zn$_{40}$ nucleus, in particular, exhibits some features of vibrational behavior. The 2_2^+ and 4_1^+ levels are nearly degenerate, at 1.759 and 1.786 MeV, respectively, with about twice the excitation energy of the 2_1^+ level at 0.885 MeV. However, the expected third member of the $0_2^+, 2_2^+, 4_1^+$ two-phonon triplet, the 0_2^+ level, lies at a much lower energy, at 1.068 MeV, and will be discussed further below.

The experimental transition probabilities represented by $B(E2)$ values are given in Table III. It is interesting to compare some of the ratios of the measured $B(E2)$ values with the corresponding predicted ratios from the vibrational model. The simple vibrational model predicts that the $B(E2)$ values from the two-phonon states ($2_2^+, 4_1^+$) to the one-phonon state (2_1^+) should be twice as large as the value of the $B(E2)$ from the one-phonon state (2_1^+) to the zero-phonon state (0_1^+). The actual experimental ratios are $B(E2; 4_1^+ \to 2_1^+)/B(E2; 2_1^+ \to 0_1^+) = 2.6(3)$ and $B(E2; 2_2^+ \to 2_1^+)/B(E2; 2_1^+ \to 0_1^+) = 0.6(1)$. The 2_2^+ state is thus seen to be less collective, from this perspective, than the 4_1^+ state; indeed, the value of the $B(E2 : 2_2^+ \to 2_1^+) = 10.0(17)$ W.u. is smaller than would be expected for a one-phonon transition in the vibrational model. Yet, the $2_2^+ \to 0_1^+$ transition, which is a forbidden two-phonon transition in the vibrational model, has only a very small $B(E2)$ value, $B(E2; 2_2^+ \to 0_1^+) = 0.58(11)$ W.u. However, new $(n, n'\gamma)$

TABLE II. Summary of the measured effects, ϵ, the experimental logarithmic slopes S of the angular correlations of the γ-emitting nuclei, and the precession angles $\Delta\theta^{\mathrm{exp}}$. The $\Delta\theta^{\mathrm{Rut}}/g$ were calculated.

E_x (MeV)	I^π	$\theta_{\mathrm{Det.}}$	θ	$|S|$ (mrad^{-1})	$\Delta\theta^{\mathrm{Exp't}}$ (mrad)	$\langle\Delta\theta^{\mathrm{Exp't}}\rangle$ (mrad)	$\Delta\theta^{\mathrm{Rut}}/g$ (mrad)	$\langle g\rangle$
0.885	2_1^+	58.3°	0.0133(8)	1.227(11)	−10.9(6)			
		73.7°	0.0192(9)	1.797(35)	−10.7(6)			
						−10.8(4)	−28.2[a]	+0.38(2)
1.759	2_2^+	58.3°	0.0145(100)	1.169(61)	−12.4(86)			
		73.7°	0.0197(118)	1.617(183)	−12.2(75)			
						−12.3(56)	−26.1	+0.47(22)
1.786	4_1^+	58.3°	0.0075(34)	0.77(7)	−9.7(45)			
		73.7°	0.0079(53)	0.78(8)	−9.8(68)			
						−9.7(37)	−26.1	+0.37(14)

[a]The linear TF parametrization with an attenuation factor $G_{\mathrm{beam}} = 0.59(5)$ [11] yields essentially the same $\Delta\theta/g$, namely $\Delta\theta/g(2_1^+) = 28.9(25)$ mrad.

measurements [25] may yield additional information about the multipolarity of the $2_2^+ \rightarrow 2_1^+$ transition.

Thus, overall, the ^{70}Zn data do exhibit some of the characteristics of a vibrational nucleus. Within this model the g factors of vibrational states in ^{70}Zn are predicted to have the collective value $g = Z/A = +0.429$. The systematics of the g factors of the 2_1^+ and 4_1^+ states for the Zn isotopes from $N = 34$ to $N = 42$, shown in Fig. 7, are in fair agreement, within experimental errors, with this prediction.

A spherical shell-model perspective is expected to provide a more microscopic description of the low-lying states in ^{70}Zn. As noted in Sec. I, a simple picture for $^{70}_{30}$Zn$_{40}$ is that of a closed, inert, neutron fp shell and a closed, inert, $f_{7/2}$ proton subshell plus two protons in the $p_{3/2}$ orbital. In this configuration a 2^+ state, whose Schmidt g-factor value would be $g(p_{3/2})_\pi = +2.529$ (much larger than the measured value), can be formed, but not a 4^+ state. Nucleon excitations, within the framework of the shell model, must be considered. Therefore, large-scale shell-model calculations were carried out in two distinct spaces, as described below. By comparing their results with the experimental values it becomes possible to determine whether the measured properties of the low-lying states of ^{70}Zn result mostly from proton excitations within the fp shell, or from both neutron (primarily) and proton excitations to the $g_{9/2}$ orbital, thus indicating the softness of the $N = 40$ subshell closure.

The first set of calculations used the computer code ANTOINE [26], assumed a closed, inert, $^{40}_{20}$Ca$_{20}$ core, and used the full fp shell-model space. Thus, only proton excitations within the fp shell were involved, from the $f_{7/2}$ and $p_{3/2}$ orbitals. The commonly-used effective charges $e_p = 1.5e$ and $e_n = 0.5e$ were used, as well as the free nucleon g factors [$g(s)_p = +5.586$, $g(s)_n = -3.826$ and $g(l)_p = +1$, $g(l)_n = 0$]. Three different interactions, commonly used for fp nuclei were used, FPD6 [27], KB3 [28], and GXPFA [29]. The calculational results are summarized in Table III (for $B(E2)$ values), Table IV (for excitation energies), and Table V (for g factors), and in each table they are compared with the experimental data.

Tables III, IV, and V show the limitations of the full fp large-scale shell-model calculations; namely it is clear that, regardless of the specific interaction chosen, the low-lying states in ^{70}Zn involve more than just proton excitations in the fp shell. The calculated g factors with the FPD6, KB3, and GXPFA interactions in the full fp space are much larger than the experimental values. None of the three interactions comes close to predicting either all the $B(E2)$ values or all the excitation energies observed.

Therefore, another large-scale shell-model calculation that included the $g_{9/2}$ orbital was carried out. This calculation assumed a closed, inert, $^{56}_{28}$Ni$_{28}$ core and used, for both neutrons and protons, the $p_{3/2} f_{5/2} p_{1/2} g_{9/2}$ space. The effective charges and nucleon g factors were those previously used in the earlier calculations of the present article, and again the computer code ANTOINE was used. The matrix elements used in this calculation were those of the JJ4B interaction of A. F. Lisetskiy and B. A. Brown [20]. The results of these calculations are given, for each nuclear property, as the

TABLE III. Calculated and experimental $B(E2)$ values in ^{70}Zn. The calculated $B(E2)$ values are given in e^2b^2.

I_i^π	Exp't.		FPD6 fp	KB3 fp	GXPFA fp	JJ4B $p_{3/2} f_{5/2} p_{1/2} g_{9/2}$
	(W.u.)	(e^2b^2)				
$2_1^+ \rightarrow 0_1^+$	16.5(9)	0.028(2) [1]	0.0110	0.00868	0.00811	0.0205
$2_2^+ \rightarrow 0_1^+$	0.58(11)	0.0010(2)[a]	0.00049	0.00270	0.00301	0.0002
$2_2^+ \rightarrow 2_1^+$	10.0(17)	0.017(3) [a]	0.00034	0.01226	0.00255	0.0170
$4_1^+ \rightarrow 2_1^+$	42(4)	0.072(7)	0.00186	0.00248	0.00242	0.0281

[a]Branching and mixing ratios, $(2_2^+ \rightarrow 2_1^+) = 59.5\%$, $(2_2^+ \rightarrow 0_1^+) = 40.5\%$ and $\delta = 0.75(15)$ were taken from Ref. [15].
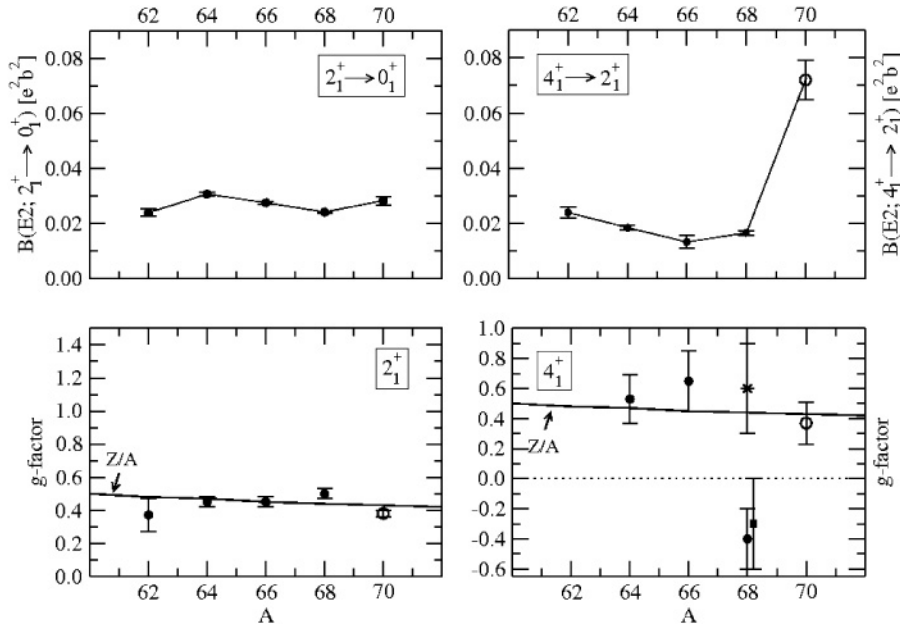
FIG. 7. Experimental g factors of 2_1^+ and 4_1^+ states, and $B(E2)$ values of corresponding transitions in units of e^2b^2, are displayed as functions of the mass number A of the even Zn nuclei. The closed circles and the square refer to previous measurements using scintillators and Ge detectors, respectively [1,3,4,13]; the open circles represent the present results. The star refers to Ref. [5]. The connecting lines are drawn to guide the eye. The negative $g(4_1^+)$ reported in Refs. [3,13] does not fit the systematics and requires further scrutiny.

last column in Tables III, IV, and V. The agreement with experiment is now much better, highlighting the vital role that is played by neutron excitations to the $g_{9/2}$ orbital. The measured $B(E2)$ values are better reproduced in Table III. The small measured $B(E2; 2_2^+ \rightarrow 0_1^+)$ is well accounted for. The calculated excitation energies in Table IV are all within 0.217 MeV of the experimental ones. The calculated g factors in Table V are also closer to experiment.

For both protons and neutrons, in the present calculation, the $f_{5/2}$, $p_{1/2}$, and $g_{9/2}$ single-particle energies that were used were higher than the $p_{3/2}$ single-particle energy by 0.3707, 1.3871, and 3.7622 MeV, respectively. It was noted in Ref. [8] that the results of calculations that include the $g_{9/2}$ orbital are sensitive to the input value of the energy difference between the $g_{9/2}$ and $p_{1/2}$ single-particle levels. In the present calculation a value of 2.37 MeV was used for both protons and neutrons. The wave functions that emerge in the present calculation are very fragmented; the 0_1^+, 2_1^+, 2_2^+, and 4_1^+ wave functions all have at least 25 different shell-model configuration components of over 1% intensity, but no component is as large as 10% in intensity. This fragmentation suggests that the structure of ^{70}Zn approaches that of a collective system with wave functions that incorporate many spherical shell-model configurations. A detailed study of the wave functions suggests that on average between three to four neutrons, but less than 0.13 protons, are excited to the $g_{9/2}$ orbital. Such proton excitations are

therefore less important for ^{70}Zn than is suggested in Ref. [8] for its isotone ^{72}Ge.

In the JJ4B calculations the 0_2^+ state lies at 1.632 MeV compared to the observed value of 1.070 MeV. The calculated $B(E2)$ values are 0.0092 e^2b^2 (5.4 W.u.) for the $0_2^+ \rightarrow 2_1^+$ transition and 0.00015 e^2b^2 (0.09 W.u.) for the $2_2^+ \rightarrow 0_2^+$ transition. In the vibrational model the former is a one-phonon transition and the latter a zero-phonon transition. One possible reason for the relatively low 0_2^+ excitation energy is that, in the results of the shell-model calculation with the JJ4B interaction, the 0_2^+ state has about one neutron less in the higher lying $g_{9/2}$ orbital than the 0_1^+, 2_1^+, 2_2^+, and 4_1^+ states.

The JJ4B calculations were repeated with the larger than commonly used effective charges of $e_p = 1.76e$ and $e_n = 0.97e$ that were used in the calculation SMII of Ref. [7]. All the calculated $B(E2)$ values in the last column of Table III were then approximately doubled. The new calculated values overpredict the experimentally measured $B(E2)$ values of the $2_1^+ \rightarrow 0_1^+$ and the $2_2^+ \rightarrow 2_1^+$ transitions. However, the new value of 0.0594 e^2b^2 agrees better with, but still underestimates, the large experimental $B(E2)$ value for the $4_1^+ \rightarrow 2_1^+$ transition.

The JJ4B calculations for the g factors were also repeated, using the free nucleon g_l factors and, as in Ref. [1], the quenched, effective nucleon g_s factors of $(g_s)_{\text{eff}} = 0.75(g_s)_{\text{free}}$. The resulting calculated g factors, $g(2_1^+) = +0.305$, $g(2_2^+) =$

TABLE IV. Calculated and experimental excitation energies E_x (I), in MeV, in ^{70}Zn.

I_i^π	Exp't.	FPD6 fp	KB3 fp	GXPFA fp	JJ4B $p_{3/2}f_{5/2}p_{1/2}g_{9/2}$
2_1^+	0.885	1.590	1.056	1.051	0.957
2_2^+	1.759	2.175	3.317	3.901	1.975
4_1^+	1.786	1.812	5.825	3.640	1.869

TABLE V. Calculated and experimental $g(I)$ factors in ^{70}Zn.

I_i^π	Exp't.	FPD6 fp	KB3 fp	GXPFA fp	JJ4B $p_{3/2}f_{5/2}p_{1/2}g_{9/2}$
2_1^+	+0.38(2)[a]	+1.52	+1.83	+1.89	+0.276
2_2^+	+0.47(22)	+1.26	+1.99	+1.53	+0.100
4_1^+	+0.37(14)	+1.12	+1.18	+1.12	+0.317

[a]A value, $g = +0.38(4)$, was obtained in Ref. [1].

$+0.134$ and $g(4_1^+) = +0.345$ were slightly larger than those in the last column of Table V.

It has thus been shown that the properties of the low-lying states of ^{70}Zn can be explained fairly well by large-scale shell-model calculations in the $p_{3/2}f_{5/2}p_{1/2}g_{9/2}$ space. Neutron excitations across the $N = 40$ barrier play an important role, indicating that the $N = 40$ subshell closure is not rigid. The results of the present work are included in Fig. 7, where the systematics of the experimental g factors and $B(E2)$ values for the even-A Zn isotopes are shown.

In summary, g factors and lifetimes of several low-lying states in ^{70}Zn have been measured and compared with the results of shell-model calculations. Although some characteristics, especially the ratios $E(4_1^+)/E(2_1^+)$ and $B(E2; 4_1^+ \rightarrow 2_1^+)/B(E2; 2_1^+ \rightarrow 0_1^+)$, suggest a vibrational structure for ^{70}Zn, the single-particle contributions are quite significant. In particular, the inclusion of neutron excitations to the $g_{9/2}$ orbital is essential to reproduce the experimental data. The large $B(E2; 4_1^+ \rightarrow 2_1^+)$ value could not be explained within the framework of the shell model, with the spaces that were used, even with large effective charges; however, this value fits well with the vibrational model.

[1] O. Kenn, K.-H. Speidel, R. Ernst, S. Schielke, S. Wagner, J. Gerber, P. Maier-Komor, and F. Nowacki, Phys. Rev. C **65**, 034308 (2002).

[2] J. Leske, K.-H. Speidel, S. Schielke, O. Kenn, J. Gerber, P. Maier-Komor, S. J. Q. Robinson, A. Escuderos, Y. Y. Sharon, and L. Zamick, Phys. Rev. C **71**, 044316 (2005).

[3] J. Leske, K.-H. Speidel, S. Schielke, J. Gerber, P. Maier-Komor, T. Engeland, and M. Hjorth-Jensen, Phys. Rev. C **72**, 044301 (2005).

[4] J. Leske, K.-H. Speidel, S. Schielke, J. Gerber, P. Maier-Komor, T. Engeland, and M. Hjorth-Jensen, Phys. Rev. C **73**, 064305 (2006).

[5] P. Boutachkov, N. Benczer-Koller, G. J. Kumbartzki, A. Escuderos, Y. Y. Sharon, L. Zamick, S. J. Q. Robinson, H. Ai, M. Chamberlain, G. Gürdal *et al.*, Phys. Rev. C **75**, 021302(R) (2007).

[6] O. Perru, O. Sorlin, S. Franchoo, F. Azaiez, E. Bouchez, C. Bourgeois, A. Chatillon, J. Daugas, Z. Dlouhy, Z. Dombradi *et al.*, Phys. Rev. Lett. **96**, 232501 (2006).

[7] J. V. de Walle, F. Aksouh, F. Ames, T. Behrens, V. Bildstein, A. Blazhev, J. Cederkäll, E. Clément, T. E. Cocolios, T. Davinson *et al.*, Phys. Rev. Lett. **99**, 142501 (2007).

[8] M. Hasegawa, T. Mizusaki, K. Kaneko, and Y. Sun, Nucl. Phys. **A789**, 46 (2007).

[9] V. Werner, N. Benczer-Koller, G. Kumbartzki, J. D. Holt, P. Boutachkov, E. Stefanova, M. Perry, N. Pietralla, H. Ai, K. Alexandrova *et al.*, Phys. Rev. C **78**, 031301(R) (2008).

[10] N. Benczer-Koller and G. J. Kumbartzki, J. Phys. G: Nucl. Part. Phys. **34**, R321 (2007).

[11] K.-H. Speidel, O. Kenn, and F. Nowacki, Prog. Part. Nucl. Phys. **49**, 91 (2002).

[12] N. Benczer-Koller, M. Hass, T. M. Brennan, and H. T. King, J. Phys. Soc. Jpn. **44**, 341 (1978).

[13] J. Leske, K.-H. Speidel, S. Schielke, O. Kenn, D. Hohn, J. Gerber, and P. Maier-Komor, Phys. Rev. C **71**, 034303 (2005).

[14] P. Boutachkov, S. J. Q. Robinson, A. Escuderos, G. Kumbartzki, N. Benczer-Koller, E. Stefanova, Y. Y. Sharon, L. Zamick, E. A. McCutchan, V. Werner *et al.*, Phys. Rev. C **76**, 054311 (2007).

[15] J. K. Tuli, Nucl. Data Sheets **103**, 389 (2004).

[16] H. Ohm, M. Liang, G. Molnár, S. Raman, K. Sistemich, and W. Unkelbach, Phys. Lett. **B241**, 472 (1990).

[17] T. Kibédi and R. H. Spear, At. Data Nucl. Data Tables **80**, 35 (2002).

[18] A. Poves, J. Sanchez-Solano, E. Caurier, and F. Nowacki, Nucl. Phys. **A694**, 157 (2001).

[19] M. Hjorth-Jensen, T. Kuo, and E. Osnes, Phys. Rep. **261**, 125 (1995).

[20] A. F. Lisetskiy and B. A. Brown (private communication).

[21] A. Piqué, J. M. Brennan, R. Darling, R. Tanczyn, D. Ballon, and N. Benczer-Koller, Nucl. Instrum. Methods Phys. Res. A **279**, 579 (1989).

[22] X-Ray Instrumentation Associates: http://www.xia.com/.

[23] J. C. Wells and N. R. Johnson, *Computer code LINESHAPE* (1999), PD-LNL version.

[24] N. K. B. Shu, D. Melnik, J. M. Brennan, W. Semmler, and N. Benczer-Koller, Phys. Rev. C **21**, 1828 (1980).

[25] D. Mücher, S. W. Yates *et al.* (to be published).

[26] E. Caurier, computer code ANTOINE, IReS, Strasbourg (1989–2004).

[27] W. Richter, M. van der Merwe, R. Julies, and B. Brown, Nucl. Phys. **A523**, 325 (1991).

[28] A. Poves and A. Zuker, Phys. Rep. **70**, 235 (1981).

[29] M. Honma, T. Otsuka, B. A. Brown, and T. Mizusaki, Phys. Rev. C **69**, 034335 (2004).